Article

Biomechanical Effects of Deep Anterior Lamellar Keratoplasty and Penetrating Keratoplasty for Keratoconus: A Finite Element Analysis

Hua Li[1], Min Chen[2,3], Qingjun Zhou[2,3], Xiaojing Pan[2,3], Jun Cheng[2,3], Lin Cong[2,3], Ting Zhang[2,3], Yanling Dong[2,3], and Lixin Xie[2,3]

[1] Department of Ophthalmology, Shanghai Ninth People's Hospital, Shanghai Jiaotong University School of Medicine, Shanghai, China
[2] State Key Laboratory Cultivation Base, Shandong Provincial Key Laboratory of Ophthalmology, Shandong Eye Institute, Shandong First Medical University and Shandong Academy of Medical Sciences, Qingdao, China
[3] Qingdao Eye Hospital of Shandong First Medical University, Qingdao, China

Purpose: To theoretically compare corneal displacement and the von Mises (VM) stress distribution of deep anterior lamellar keratoplasty (DALK) and penetrating keratoplasty (PK) for keratoconus (KC) and to evaluate the effects of residual stromal thickness (RST) and intraocular pressure (IOP) on postoperative corneal biomechanics.

Methods: We performed DALK and PK simulations using Ansys by employing anisotropic nonlinear hyperelastic corneal material properties. We analyzed corneal displacement and VM stress in DALK and PK models under IOPs of 10, 15, 20, and 25 mmHg. We established two DALK models: The ideal-type DALK ensured that postoperative central corneal thickness was constant at 560 µm and the corneal graft thickness varied with RST. The clinical-type DALK ensured that corneal grafts had the same thickness (500 µm) regardless of RST. Then we analyzed the effects of RST and IOP on postoperative corneal displacement and VM stress.

Results: Corneal displacement and VM stress were lower in the DALK than in the PK model. In the ideal-type DALK model, an increase in RST was associated with increased deformation and decreased VM stress in the healing zone, except for a RST of 0 µm. In the clinical-type DALK model, deformation and VM stress in the healing zone decreased with an increase in RST, except for a RST of 0 µm.

Conclusions: DALK showed more stability than PK. For the ideal-type DALK model, an increase in RST resulted in decreased postoperative corneal biomechanics in the healing zone. For the clinical-type DALK model, corneal deformation and VM stress decreased with an increase in RST, which provides numerical evidence for the design of corneal transplantation for patients with KC.

Translational Relevance: In this computational modeling study, we first theoretically compared corneal biomechanics between DALK and PK for KC. Then, the effects of RST and IOP on postoperative corneal biomechanics were investigated. Our findings provide novel insights into the optimal design for corneal transplantation for patients with KC.

Introduction

Keratoconus (KC) is a progressive, non-inflammatory disorder characterized by thinning and protrusion of the central or paracentral cornea, with consequent irregular myopic astigmatism. X-ray diffraction studies have indicated that the collagen fiber network in patients with KC is disorganized and lacks uniform orientation.[1,2] Collagen fibril arrangement and density in the stroma are primary contributors to corneal biomechanical stiffness. Localized corneal thinning and reduced corneal elastic modulus affect KC protrusion.[3] Biomechanical studies have

1

demonstrated that the elastic modulus of KC is reduced by 50% to 60% compared with normal corneas.[4,5]

Appropriate treatments for KC should be designated based on KC progression; for patients with severe KC or those for whom nonsurgical treatments fail to achieve acceptable visual acuity, deep anterior lamellar keratoplasty (DALK) and penetrating keratoplasty (PK) are the most frequent surgical options.[6] Two types of DALK exist: pre-descemetic with deep stromal dissection (pd-DALK; ≥75%) and descemetic with total stromal resection (d-DALK).[6–9] The main goals of surgical treatment for KC are to improve visual acuity and enhance corneal biomechanical properties to prevent KC from reoccurring. KC may reoccur following PK or DALK, but latency is considerably longer in PK than DALK (20 years vs. 4 years).[10,11] Unfortunately, we have been unable to estimate the incidence of recurrent ectasia. There is a general consensus that d-DALK and PK are the most favorable surgical techniques for restoration of best uncorrected visual acuity for KC.[6] Ardjomand et al.[12] compared visual function after DALK and PK in 23 patients with KC and concluded that residual stromal thickness (RST) affected visual function following DALK. Specifically, KC eyes with RST less than 20 µm had visual acuity comparable to that of PK. However, other studies comparing visual acuity between pd-DALK and d-DALK have reported no significant difference in visual acuity at an average follow-up time of 30.4 months, although eyes in the d-DALK group tended to exhibit more rapid visual recovery.[7,13,14] Regarding corneal biomechanics, evidence suggests that residual stromal tissue reduces the risk of Descemet's membrane (DM) rupture[15] and prevents microperforations from progressing to macroperforations during surgery.[16]

Several studies have compared corneal biomechanics in vivo following DALK and PK using the Ocular Response Analyzer (Reichert Ophthalmic Instruments, Buffalo, NY) or Corvis ST (OCULUS, Wetzlar, Germany).[17–22] However, results have been controversial, with the majority of studies concluding that corneal biomechanical strength after DALK is more stable than that after PK,[17–19,22] whereas others have reported no difference or uncertain results.[20,21] These clinical observations do not provide a sufficient theoretical basis for evaluating postoperative corneal biomechanics as a whole. There has been a paucity of research on the effects of RST on corneal biomechanics after DALK. The finite element model (FEM) is a useful tool for providing insight into the effects of geometrical parameters on corneal deformation.[23–28] Therefore, we aimed to establish a realistic three-dimensional model of DALK and PK for KC for numerical analysis and to evaluate the effects of RST and intraocular pressure (IOP) on postoperative corneal biomechanics. This study is the first to theoretically compare corneal biomechanics between DALK and PK.

Methods

FEM Modeling of Cornea in a Computational Model

Normal Corneal Geometry

The cornea is the transparent outer covering of the eyeball that is comprised of five layers: epithelium, Bowman's membrane, stroma, Descemet's membrane, and endothelium.[29] The stroma forms approximately 90% of the entire thickness of the cornea and is the main contributor to corneal biomechanics. Unloaded normal corneas are assumed to be symmetric with a half-sphere shape at the central region and are clamped at the sclera, which provides a reasonable approximation of a healthy corneal shape.[3,30] We created corneal geometry with an idealized smooth surface and axisymmetric geometry using a spherical coordinate system. The origin of the coordinates was the vertex of the posterior corneal surface. Figure 1A details the dimensions of the corneal geometric model, which were based on previously published data.[3,31] Hyperelastic material behavior was supported in Ansys 18.0 (Ansys, Inc., Canonsburg, PA) for shell, plane, and solid elements. We applied solid elements with eight nodes (Ansys SOLSH190) in consideration of the limitations of the shell elements in the Ansys application of boundary conditions. This solid element simulates shell structures of various thicknesses and possesses analytical characteristics such as plasticity, hyperelasticity, stress stiffening, creep, large deformation, and large strain. It is able to simulate the behavior of almost incompressible and completely incompressible elastic–plastic materials. Because corneal biomechanics is depth dependent,[32] we divided the normal cornea into 12 element layers in the depth direction as follows. We modeled the epithelium and Bowman's membrane as a layer of elements with a constant thickness of 45 µm. We modeled the DM and endothelium as a layer of elements with a constant thickness of 15 µm, which contributes minimally to corneal biomechanical properties. We divided the corneal stroma (500 µm) equally into 10 layers. We created a hexahedral mesh for all geometric parts using HyperMesh 2017.2 (Altair Engineering, Troy, MI), resulting in approximately 206,200 elements, including 157,200 for the normal cornea and 49,000 for the sclera (Fig. 1B).
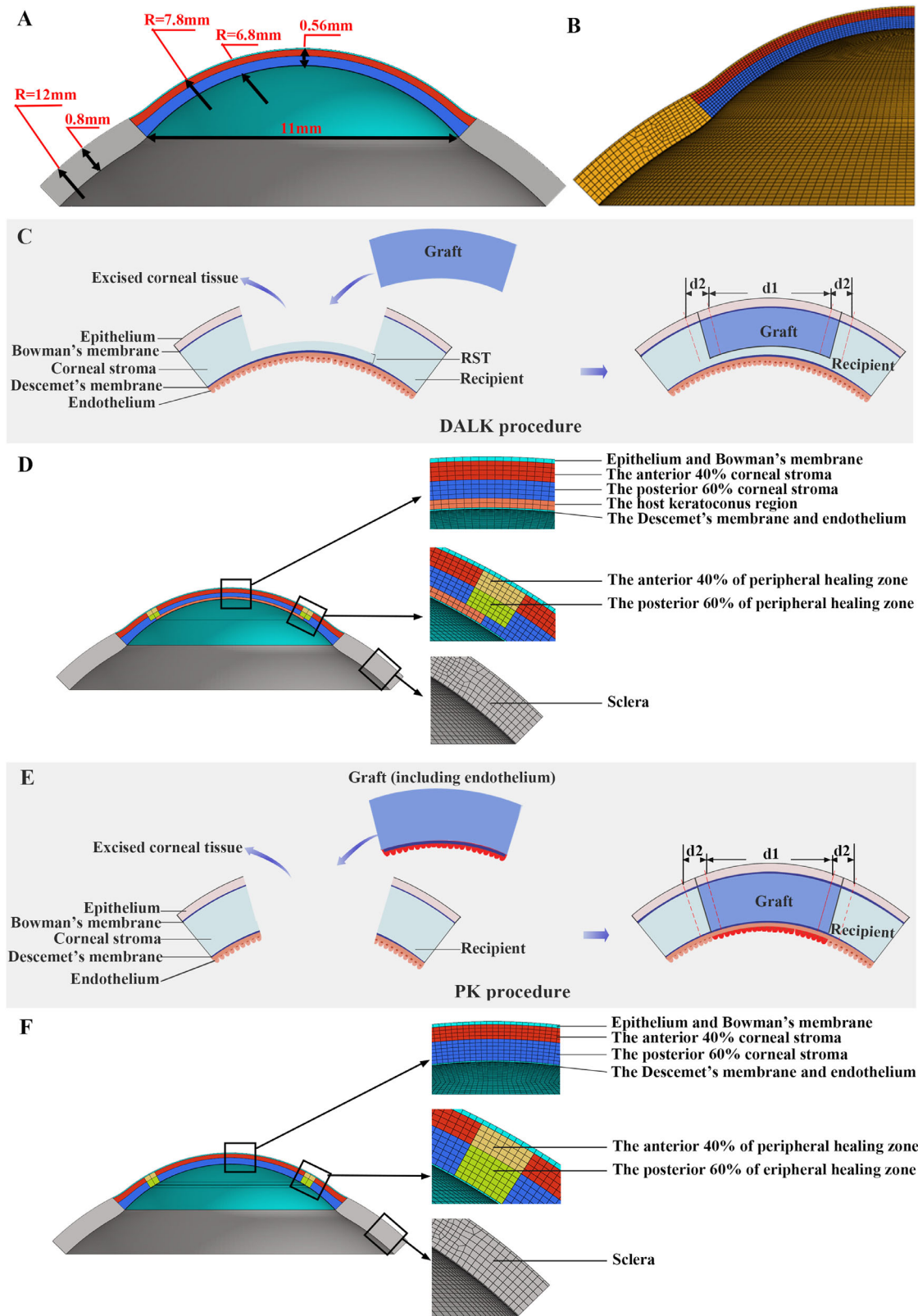
Figure 1. Geometry and FEM of the normal cornea, DALK, and PK. (**A**) Geometry of the normal cornea. (**B**) FEM of the normal cornea. (**C**) Schematic of the DALK procedure. (**D**) FEM of DALK. (**E**) Schematic of PK procedure. (**F**) FEM of PK.

Table. Constitutive Parameter Settings for Each Layer of Cornea

Corneal Tissue Partition	Constitutive Equation	Material Parameters	
		μ	α
Epithelium, endothelium, and Bowman's membrane	Ogden first-order	0.0054100	110.4
Anterior 40% corneal stroma	Ogden first-order	0.0718310	110.4
Posterior 60% corneal stroma	Ogden first-order	0.0422790	110.4
Anterior 40% of peripheral healing zone	Ogden first-order	0.0359160	110.4
Posterior 60% of peripheral healing zone	Ogden first-order	0.0211400	110.4
Sclera	Ogden first-order	0.2709105	150.0
Keratoconus region	Ogden first-order	0.0232535	110.4

Corneal Material Properties

Following creation of the geometry, we assigned material properties and boundary conditions to the model. Corneal biomechanical properties are complex and exhibit nonlinear, anisotropic, viscoelastic, and creep behaviors.[33–35] We designated the cornea as an anisotropic, hyperelastic, and nearly incompressible material in the FEM to improve computational efficiency based on previous modeling by Khan et al.,[25] Kling and Marcos,[28] Pandolfi and Manganiello,[36] and Elsheikh and Wang.[37] Corneal biomechanics is depth dependent, and tensile strength in the anterior stroma is nearly twice that of the posterior stroma.[32] To model corneal mechanical behavior, we employed a first-order hyperelastic Ogden material model:[25,30,38]

$$W = \sum_{i=1}^{N} \frac{\mu_i}{\alpha_i} \left(\bar{\lambda}_1^{\alpha_i} + \bar{\lambda}_2^{\alpha_i} + \bar{\lambda}_3^{\alpha_i} - 3 \right) + \sum_{k=1}^{N} \frac{1}{D_k}(J-1)^{2k}$$

(1)

where $\bar{\lambda}_1$, $\bar{\lambda}_2$, and $\bar{\lambda}_3$ represent the deviatoric principal stretches $= J^{-1/3}\lambda_k$ ($k = 1, 2, 3$); λ_1, λ_2, and λ_3 are the principal stretches; $J = \lambda_1\lambda_2\lambda_3$; and α, μ, and D are the material constants. D is a compressibility parameter whose value depends on Poisson's ratio (ν). The reported values of ν ranged from 0.45 to 0.50,[27,39,40] and we assumed a value of 0.49 in this study. Constitutive parameters α and μ indicate the material constants representing the strain-hardening exponent and shear modulus, respectively, according to a previous study (Table).[41]

FEM Modeling of DALK

Figure 1C presents a schematic of DALK surgery. The graft diameter ($d_1 + 0.5$ mm) was 7.75 mm. The healing zone diameter (d_2) was 0.5 mm and was comprised of the graft and recipient, each constituting 0.25 mm. We applied binding contact elements in graft-recipient modeling. We assumed two distinct zones in the DALK model (Fig. 1D), including healing and non-healing zones. We divided the healing zone into two parts in the direction of depth (anterior 40% and posterior 60%). Based on previous studies,[42] we reduced the material parameters (α, μ) in the healing zone by 50% compared with the normal cornea. The central non-healing zone was composed of five parts in the direction of depth, including the epithelium and Bowman's membrane, the anterior 40% and posterior 60% of the corneal stroma, host KC region, DM, and endothelium. We estimated the diameter of the KC region with weak corneal biomechanical strength to be 7 mm.[26] We decreased the material parameters (α, μ) by 50% in accordance with ex vivo evidence of a 50% to 60% decrease in elastic modulus in KC corneas.[4,5] The two DALK model schemes, ideal-type and clinical-type, are described below.

Ideal-Type DALK

The ideal-type DALK ensured that postoperative corneal thickness remained constant at 560 μm, with the goal of achieving a final corneal shape approximating the physiological curvature of the normal cornea. The thickness of the corneal graft (500, 450, 400, 350, and 300 μm) varied with RST (0, 50, 100, 150, and 200 μm) (Supplementary Fig. S1A). Due to the limited technology available for accurate fabrication of grafts with various corneal thicknesses, we defined this model as the ideal-type DALK.

Clinical-Type DALK

We defined clinical-type DALK as corneal grafts of the same thickness (500 μm) in the clinic, regardless of variability in RST in the host cornea (0, 50, 100, 150, and 200 μm) (Supplementary Fig. S1B). Clinical optical coherence tomography results of DALK (Supplementary Fig. S2) indicated that the posterior surface of the cornea had a downward convex under the action of sutures and the posterior surface
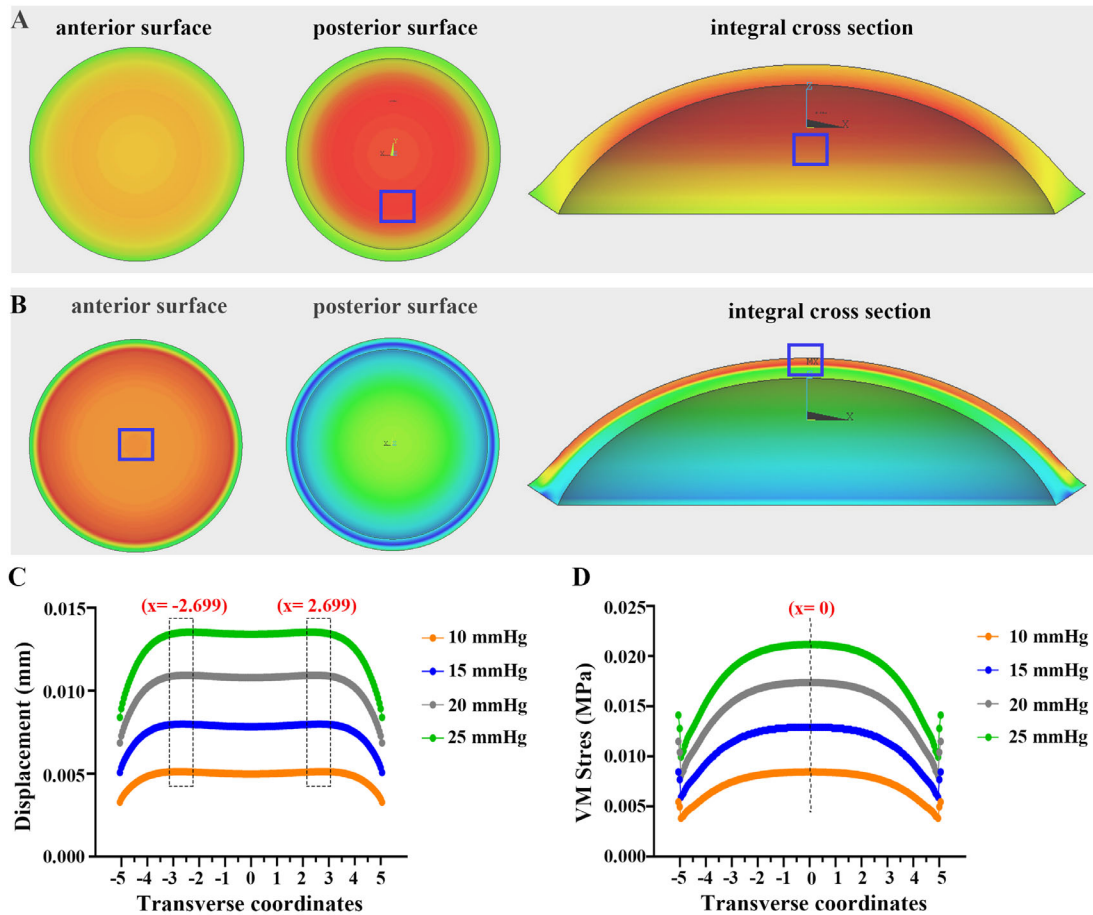
Figure 2. Displacement and VM stress distribution of the normal cornea under different IOPs. (**A**) Displacement of the normal cornea on the anterior surface, posterior surface, and integral cross section. (**B**) VM stress of the normal cornea on the anterior surface, posterior surface, and integral cross section. (**C, D**) Displacement and VM stress intensity plotted at the central section of the posterior surface of the normal cornea along the radius of the cornea.

transitioned smoothly during modeling when graft-recipient thickness exceeded host corneal thickness.

FEM Modeling of PK

Figure 1E presents a schematic of PK surgery. The graft diameter ($d_1 + 0.5$ mm) was 7.75 mm. The healing zone diameter (d_2) was 0.5 mm and was composed of the graft and recipient, each comprising 0.25 mm. We applied binding contact elements in graft-recipient modeling. We assumed two distinct zones in the PK model (Fig. 1F): healing and non-healing. We divided the healing zone into two parts in the direction of depth (anterior 40% and posterior 60%). Similar to those for DALK, material parameters (α, μ) in the PK healing zone were reduced by 50%. The central non-healing zone was composed of four parts in the direction of corneal depth, including the epithelium and Bowman's membrane, anterior 40% and posterior 60% of the corneal stroma, DM, and endothelium.

Results

Displacement and Von Mises Stress Distribution of Normal Cornea Under Different IOPs

Figure 2A depicts the displacement distribution of the normal cornea under physiological IOP (15 mmHg). The maximum deformation was 0.008016 mm and was located on the posterior surface of the corneal stroma, as indicated in the blue box. Figure 2B depicts the von Mises (VM) stress distribution in the normal cornea under physiological IOP (15 mmHg). The maximum VM stress was 0.018678 MPa and was located in the anterior 40% of the corneal stroma, as depicted in the blue box. Deformation and stress distribution trends were consistent under other IOPs (10, 20, and 25 mmHg).

Figures 2C and 2D depict the displacement and VM stress intensity plotted at the central section of the posterior surface of the normal cornea along the corneal radius. This calculation is extracted from the elements at the junction of the corneal stroma and the DM, because the VM stress of corneal endothelium is very small and it is difficult to compare the difference between groups (DALK and PK are the same position). Herein, the cornea exhibited greater deformability at higher IOP values. The VM stress calculated in this study was of the same magnitude as that reported by Gefen et al.[3] and Pandolfi et al.[43]

Displacement and VM Stress Distribution of Ideal-Type DALK

The values and coordinates of maximal corneal deformation and VM stress following ideal-type DALK are presented in Supplementary Table S1. We selected a typical model with a RST of 50 μm for analysis to examine the effects of IOP on deformation and VM stress. Figure 3A depicts the corneal central posterior surface (Fig. 3A-a), graft slave surface (Fig. 3A-b), and recipient master surface (Fig. 3A-c) as primary locations for assessing deformation and stress. Figure 3B depicts the displacement distribution of the ideal-type DALK (RST = 50 μm) under physiological IOP (15 mmHg). The maximal deformation was 0.009556 mm and was located on the posterior surface of the corneal stroma, as depicted in the blue box. Figure 3C depicts the VM stress distribution of the ideal-type DALK (RST = 50 μm) under IOP (15 mmHg). The maximal VM stress was 0.020596 MPa and was located on the anterior surface of the corneal stroma, as indicated in the blue box. Maximal deformation and VM stress were located on the posterior and anterior surfaces of the corneal stroma, respectively, for other RSTs (0, 100, 150, and 200 μm) and IOPs (10, 20, and 25 mmHg). The position of maximal VM stress moved toward the corneal center as RST increased (Supplementary Table S1).

Figures 3D and 3E depict the displacement and VM stress intensity plotted at the central section of the posterior surface after ideal-type DALK (RST = 50 μm) along the corneal radius under different IOPs. The cornea exhibited greater deformability at higher IOP values. The coordinates of the maximal deformation were (0.00, –3.47, –0.96) and were located within the coordinates of the graft-recipient healing zone (*x/y*: 3.39–3.85). The coordinates of the maximal VM stress were (0.13, –4.19, –0.70) and were located outside of the graft-recipient healing zone (*x/y*: 3.39–3.85).

Figures 3F and 3G depict the VM stress intensity plotted at the surface of the graft (slave surface) and recipient (master surface). The values of VM stress exceeded 0, indicating that the graft was close to the implant bed and increased with IOP.

Effects of RST on Displacement and VM Stress of Ideal-Type DALK

Figures 4A and 4B depict the displacement and VM stress of the posterior corneal surface after ideal-type DALK with different RSTs (0, 50, 100, 150, and 200 μm) under physiological IOP (15 mmHg). Figures 4A-a and 4A-b depict the amplification views of the healing and optical zones, respectively. In the ideal-type DALK model, a thicker RST produced greater deformation in the healing zone (Fig. 4A-a). In the optical zone, deformation trends were consistent. We observed the greatest deformation with a RST of 200 μm and the least deformation with a RST of 50 μm (Fig. 4A-b). Regarding VM stress, in the healing zone, with the exception of RST of 0 μm, which had the smallest value, VM stress decreased with an increase in RST (Fig. 4B). In the optical zone, with the exception of RST of 0 μm, which had the largest value, VM stress increased with an increase in RST (Fig. 4B).

Displacement and VM Stress Distribution of Clinical-Type DALK

The values and coordinates of maximal corneal deformation and VM stress following clinical-type DALK are presented in Supplementary Table S2. To examine the effects of IOP on deformation and VM stress distribution, we selected a typical model with a RST of 50 μm for analysis. Figure 5A depicts the corneal posterior surface (Fig. 5A-a), graft slave surface (Fig. 5A-b), and recipient master surface (Fig. 5A-c) as primary locations for studying deformation and stress. Figure 5B depicts the deformation distribution of clinical-type DALK under physiological IOP (15 mmHg). The maximal deformation was 0.009499 mm and was located on the posterior surface of the corneal stroma, as indicated in the blue box. Figure 5C depicts the VM distribution of clinical-type DALK under physiological IOP (15 mmHg). The maximal VM stress was 0.020042 MPa and was located on the anterior surface of the corneal stroma, as indicted in the blue box. Maximal deformation and VM stress were located on the posterior and anterior surface of the corneal stroma, respectively, for other RSTs (0, 100, 150, and 200 μm) and IOPs (10, 20, and 25 mmHg).
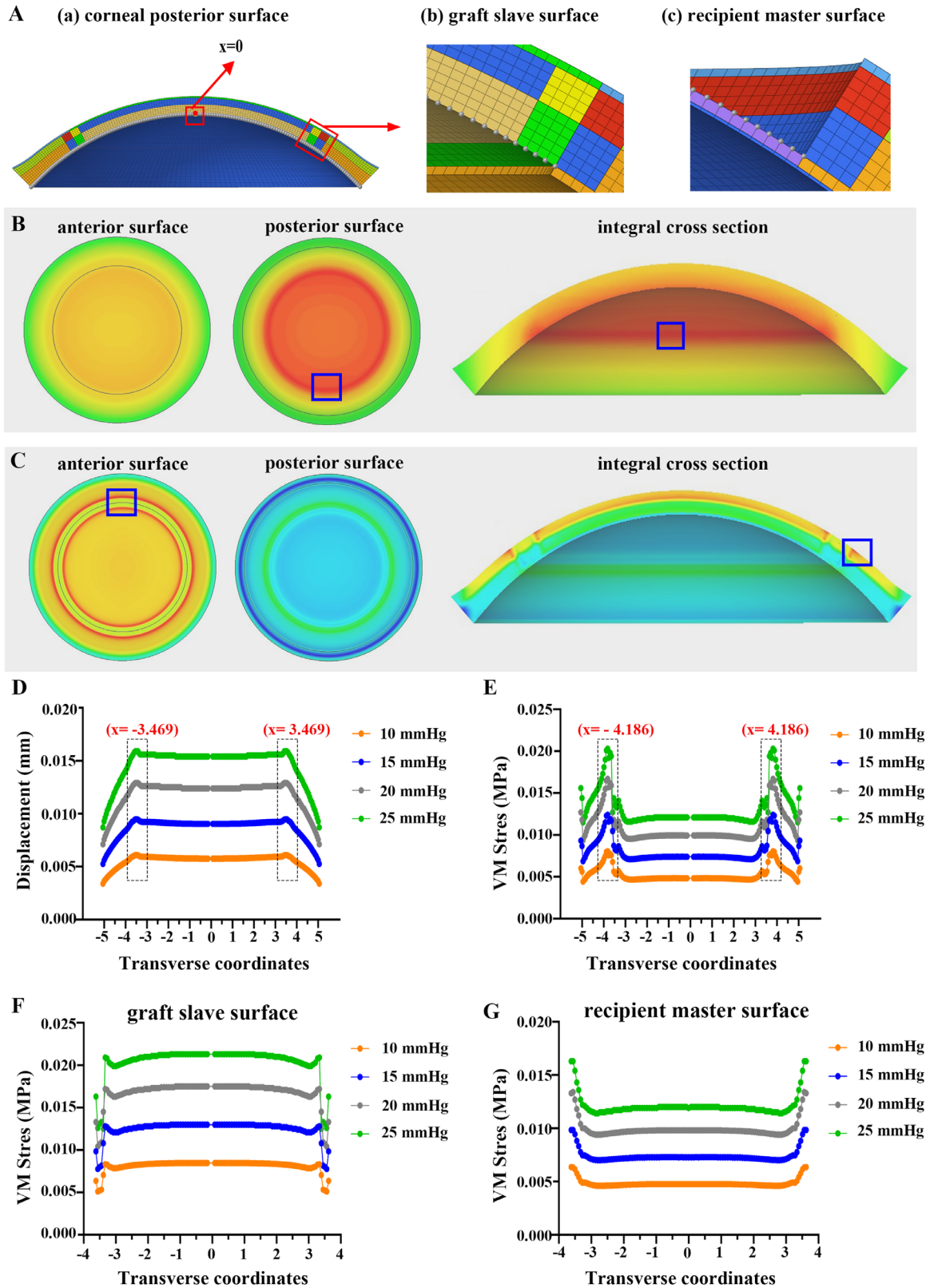
Figure 3. Deformation and VM stress distribution after ideal-type DALK with a RST of 50 μm under different IOPs. (**A**) Denotation of the central posterior corneal surface (A-a), graft slave surface (A-b), and recipient master surface (A-c) as primary locations for studying deformation and stress. (**B**) Displacement after ideal-type DALK on the anterior surface, posterior surface, and integral cross section. (**C**) VM stress after ideal-type DALK on the anterior surface, posterior surface, and integral cross section. (**D**, **E**) Displacement and VM stress intensity plotted

→

←
at the central section of the posterior surface after ideal-type DALK along the radius of the cornea. (**F**, **G**) VM stress intensity plotted at the surface of the graft (slave surface) and recipient (master surface) after ideal-type DALK.
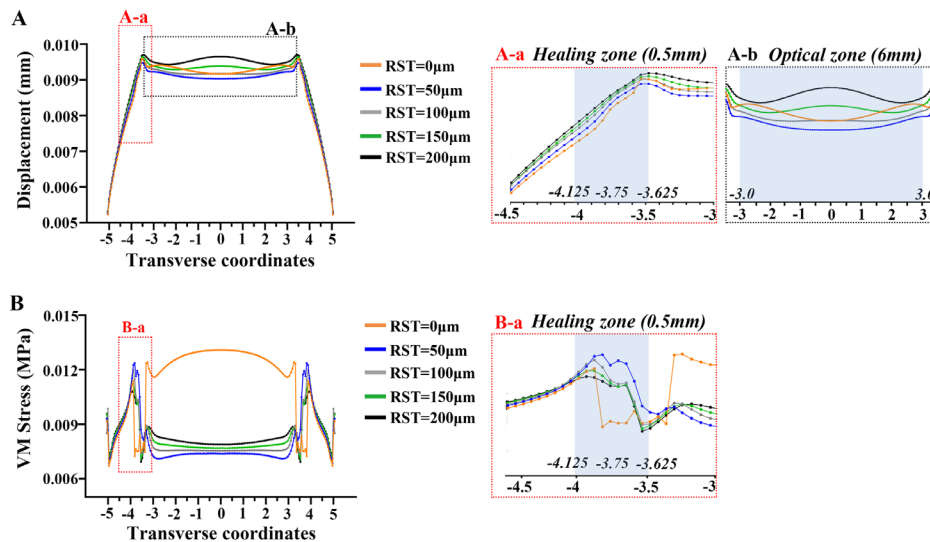
Figure 4. Effect of RST on displacement and VM stress after ideal-type DALK under IOP of 15 mmHg. (**A**) Displacement after ideal-type DALK with different RSTs under physiological IOP (15 mmHg); amplification views of the healing zone (A-a) and optical zone (A-b). (**B**) VM stress after ideal-type DALK with different RSTs under physiological IOP (15 mmHg); amplification views of the healing zone (B-a).

Figures 5D and 5E depict the displacement and VM stress intensity plotted at the central section of the posterior surface for clinical-type DALK under different IOPs. The cornea exhibited greater deformability at higher IOP values. The coordinates of the maximal deformation were (3.36, 0.98, –0.98) and were located within the coordinates of the graft-recipient healing zone (*x/y*: 3.37–3.85). The coordinates of the maximal VM stress were (–3.56, 0.00, –0.30) and were located inside the graft-recipient healing zone (*x/y*: 3.37–3.85).

Figures 5F and 5G depict the VM stress intensity plotted at the surface of the graft (slave surface) and cornea (master surface). The values of VM stress exceeded 0, indicating that the graft was close to the implant bed and increased with IOP.

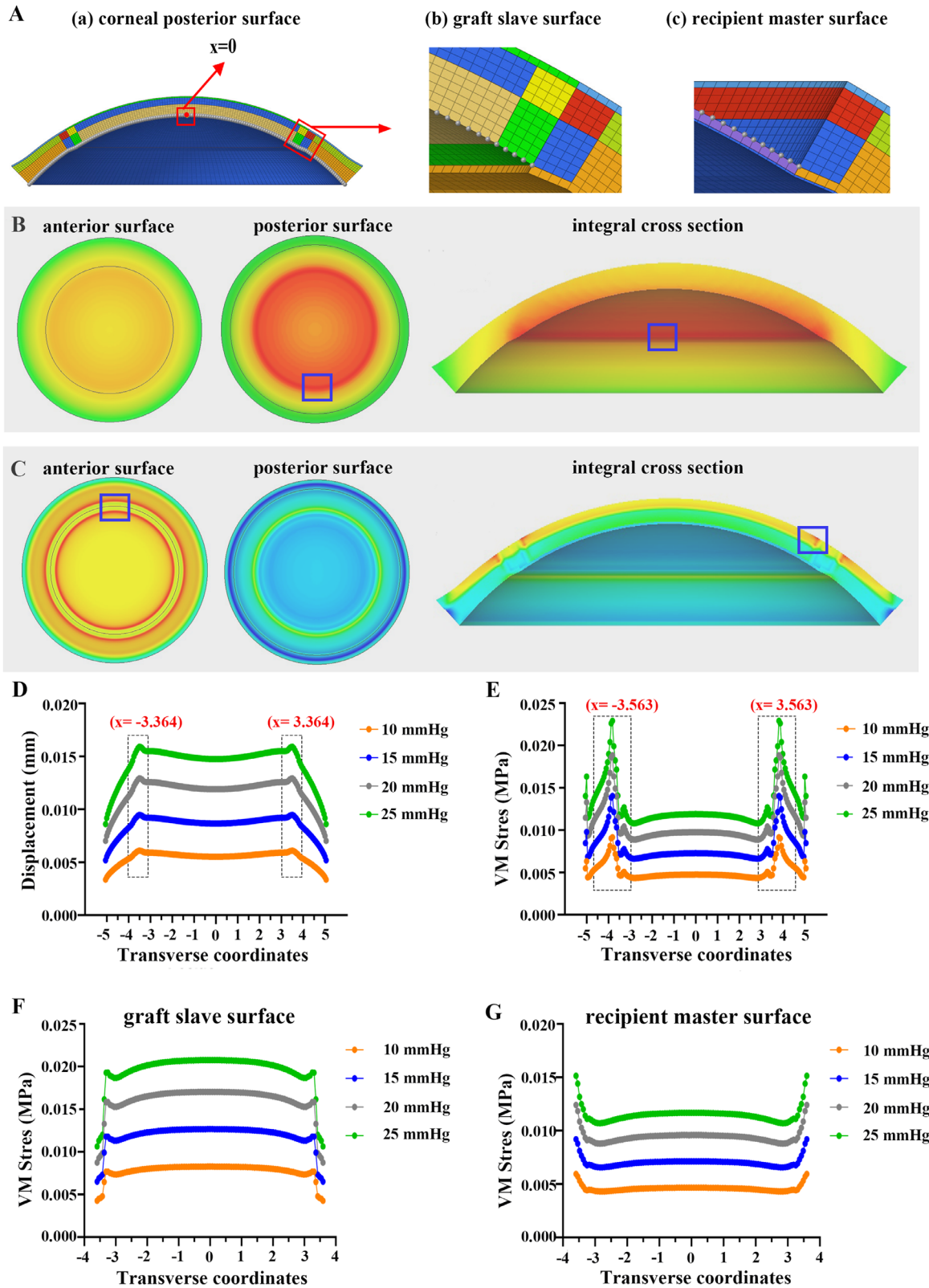## Effects of RST on Displacement and VM Stress of Clinical-Type DALK

Figures 6A and 6B depict the displacement and VM stress of the posterior corneal surface after clinical-type DALK with different RSTs (0, 50, 100, 150, and 200 μm) under physiological IOP (15 mmHg). Figures 6A-a and 6A-b depict the amplification views of the healing and optical zones (dotted line), respectively. In this model, a greater RST produced a smaller deformation in the healing zone, with the exception of RST

of 0 μm (Fig. 6A-a). In the optical zone, the deformation trends exhibited a consistent pattern; we observed the least deformation with a RST of 200 μm and greatest deformation with a RST of 0 μm (Fig. 6A-b). Regarding VM stress, with the exception of a RST of 0 μm with a large change, VM stress decreased with an increase in RST in the healing and optical zones (Fig. 6B).

Displacement and VM Stress Distribution of PK

Figure 7A depicts the displacement distribution of PK under physiological IOP (15 mmHg). The maximal deformation was 0.00985 mm and was located on the posterior surface of the corneal stroma, as indicated in the blue box. Figure 7B depicts the VM distribution of PK under physiological IOP (15 mmHg). The maximal VM stress was 0.020203 MPa and was located on the anterior surface of the corneal stroma, as indicated in the blue box. The maximal values of deformation and VM stress were located on the posterior surface and anterior surface of the corneal stroma, respectively, for other RSTs (0, 100, 150, and 200 μm) and IOPs (10, 20, and 25 mmHg).

Figures 7C and 7D depict the displacement and VM stress intensity plotted at the central section of

Figure 5. Deformation and VM stress distribution after clinical-type DALK with RST of 50 μm under different IOPs. (**A**) Denotation of the central posterior corneal surface (A-a), graft slave surface (A-b), and recipient master surface (A-c) as primary locations for studying deformation and stress. (**B**) Displacement after clinical-type DALK on the anterior surface, posterior surface, and integral cross section. (**C**) VM stress after clinical-type DALK on the anterior surface, posterior surface, and integral cross section. (**D**, **E**) Displacement and VM stress

→

←

intensity plotted at the central section of the posterior surface after clinical-type DALK along the radius of the cornea. (**F, G**) VM stress intensity plotted at the surface of the graft (slave surface) and recipient (master surface) after clinical-type DALK.
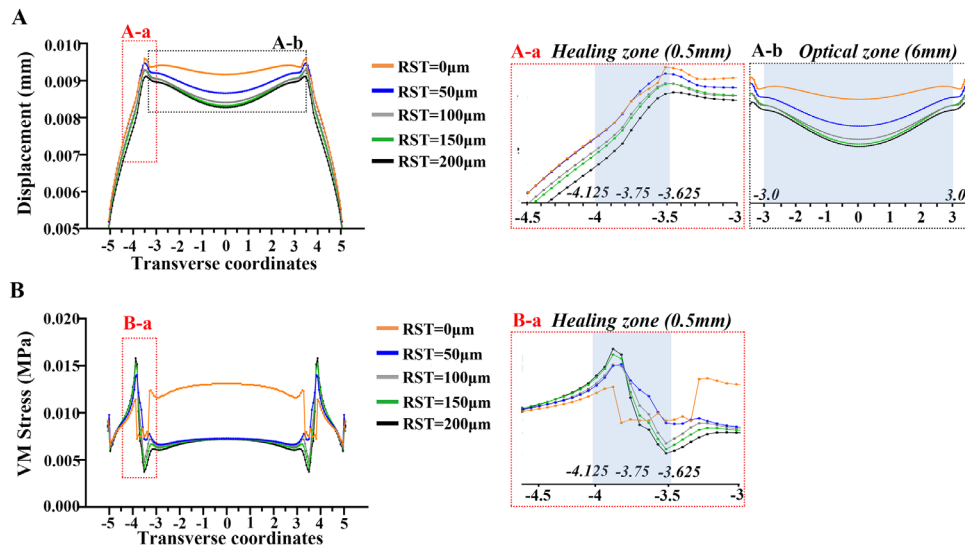
Figure 6. Influence of RST on deformation and VM stress after clinical-type DALK under IOP of 15 mmHg. (**A**) Displacement of clinical-type DALK with different RSTs under physiological IOP (15 mmHg); amplification views of the healing zone (A-a) and optical zone (A-b). (**B**) VM stress of clinical-type DALK with different RSTs under physiological IOP (15 mmHg); amplification views of the healing zone (B-a).
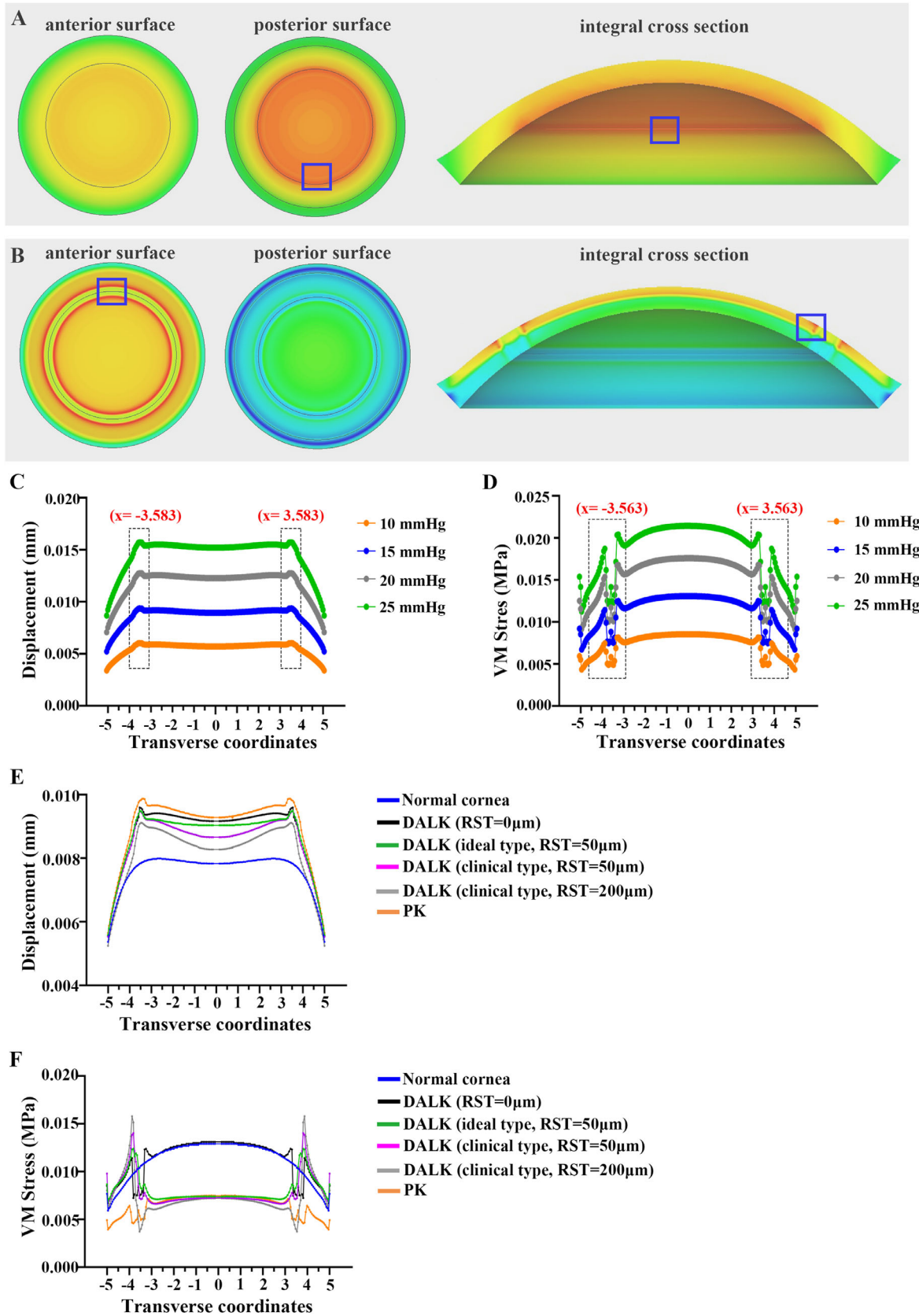
the posterior surface for PK under different IOPs. The cornea exhibited greater deformability at higher IOP values. The coordinates of the maximal deformation were (0.00, 3.58, –1.02) and were located within the coordinates of the graft-recipient healing zone (*x/y*: 3.36–3.82). The coordinates of the maximal VM stress were (3.56, 0.00, –0.35) and were located inside the graft-recipient healing zone (*x/y*: 3.36–3.82).

Comparison of Displacement and VM Stress Among DALK, PK, and Normal Cornea

Figures 7E and 7F depict the displacement and VM stress for DALK, PK, and the normal cornea. Displacement was significantly higher for PK and DALK than for the normal cornea (Fig. 7E). Displacement was higher for PK than for DALK with a RST of 0 μm, followed by ideal-type DALK with a RST of 50 μm, clinical-type DALK with a RST of 50 μm, and clinical-type DALK with a RST of 200 μm. VM stress in both healing and optical zones was lower for PK than for the normal cornea (Fig. 7F). VM stress in the healing zone was lower for DALK (including that for a RST of 0 μm), ideal-type DALK with a RST of 50 μm, and clinical-type DALK with RSTs of 50 μm and 200 μm than for the normal cornea (Fig. 7F). VM stress in the optical zone was lower for PK and DALK

than for the normal cornea, with the exception of a RST of 0 μm (Fig. 7F).

Discussion

In this study, we have presented a novel FEM for a KC patient-specific computational simulation of DALK and PK. We have provided a pilot estimate of biomechanical changes, including the effects of IOP, RST, and different surgical protocols on corneal biomechanics.

Setting of material properties is critical in FEM analysis. Histopathological analysis of KC tissue indicates a decrease in collagen lamella and mechanical failure of collagen fibers, indicative of a degradation of tissue mechanical properties.[2] In vitro biomechanical studies have demonstrated that the corneal elastic modulus of KC is reduced by 50% to 60% compared with normal corneas,[4,5] an observation that was incorporated in this study. Regarding biomechanical properties of healing tissue after corneal transplantation, wound healing in the corneal stroma restores the organization of regular collagen and forms a corneal scar.[44] The remodeling process and restoration of normal transparency occur over several years.[45] A previous study evaluated the mechanical strength of cicatrices resulting from eight corneal cataract incisions

Figure 7. Deformation and VM stress distribution after PK under different IOPs and comparison of displacement and VM stress after different surgeries. (**A**) Displacement after PK on the anterior surface, posterior surface, and integral cross section. (**B**) VM stress after PK on the

→

←

anterior surface, posterior surface, and integral cross section. (**C**, **D**) Displacement and VM stress intensity plotted at the central section of the posterior surface after PK along the radius of the cornea. (**E**) Displacement after different surgeries under physiological IOP (15 mmHg). (**F**) VM stress after different surgeries under physiological IOP (15 mmHg).

and reported that the break loads of specimens with corneal incisions were 38%, 60%, and 76% of the break loads of uninjured specimens after 1, 2, and 3 years, respectively.[42] Following DALK, the healing zone can be divided into two parts: the peripheral graft-recipient healing zone and interlamellar graft-recipient healing zone. Given that the direction of IOP is perpendicular to the cornea, we assessed only the peripheral healing zones in DALK and PK. We observed that the material parameters (α, μ) were reduced by 50%.

We considered the displacement and VM stress distribution of the normal cornea and observed that the maximal deformation (8.016 μm) occurred on the posterior surface of the cornea, whereas maximal VM stress (18.678 kPa) occurred within the anterior 40% of the corneal stromal surface. We think that the VM stress distribution was correlated with the biomechanical properties of different corneal layers and the setting of constitutive parameters for each corneal layer. In this study, we simplified the epithelium and the Bowman layer as a whole and set its biomechanical parameter μ as 0.005 in modeling, which has little effect on the biomechanical properties of the cornea as compared with the stroma layer. It is generally recognized that the corneal stroma contributes most to the overall corneal mechanical behavior. The corneal stroma biomechanics is depth dependent and the biomechanical parameters (μ) of the anterior 40% and posterior 60% corneal stroma were 0.072 and 0.042, respectively. It is well known that the greater the elastic modulus of the cornea, the greater the stress. In this normal corneal model, the anterior 40% corneal stroma has the greatest elastic modulus, so the greatest VM stress occurs here. Gefen et al.[3] also conducted a three-dimensional FEM and reported that the maximal displacement of the normal cornea was 56 μm (sevenfold larger than the value obtained in this study) and occurred at the corneal apex. The peak stress value (18.1 kPa) occurred at the corneal apex, which is consistent with our findings. In their study, the FEM considered the cornea as a transverse-orthotropic elastic material, and they selected the following values for elastic moduli of the tissues: $E_{\gamma\gamma} = 4.5$ MPa, $E_{\Psi\Psi} = 2$ MPa in the cornea and 0.7 MPa toward the sclera, and $E_{\theta\theta} = 2$ MPa in the central cornea with a gradual increase toward the periphery (up to 7 MPa in the sclera). Collectively, these findings highlight differences in the magnitude of maximum displacement in differ-ent models and parameters. Following DALK and PK, corneal stress distribution was altered, and the position of maximal VM stress shifted from the anterior 40% of the central corneal stromal surface to the anterior surface of the peripheral corneal incision. This suggests that peripheral corneal incisions after keratoplasty exhibit relatively weak corneal biomechanics, which is consistent with clinical results indicating that corneal dehiscence typically occurs at the corneal incision in keratoplasty-associated trauma.[46]

Several reports have compared corneal biomechanics following PK and DALK based on clinical observations.[17–19,22] Hosny et al.[17] and Abdelkader[22] evaluated corneal biomechanics with ocular response analyzer after PK and DALK, and they reported that the parameters corneal hysteresis and corneal resistance factor were lower in the PK group than in the DALK group. They concluded that corneas after PK have weaker biomechanical properties than normal corneas and that DALK preserves the biomechanical strength of the corneas to almost normal values. Jiang et al.[19] did a meta-analysis to evaluate the corneal biomechanics of patients who had undergone PK or DALK and reported that both corneal hysteresis and corneal resistance factor had better recovery after corneal transplantation with DALK than PK. Based on analysis with Corvis ST, Ziaei et al.[18] concluded that neither DALK nor PK could restore corneal biomechanical properties to those of healthy corneas, although PK resulted in a greater decrease in corneal biomechanical properties compared with DALK. In contrast, Maeda et al.[20] and Jafarinasab et al.[21] reported a lack of difference or uncertain results between PK and DALK corneal biomechanics. Our FEM analysis further demonstrated that displacement was higher after PK than after DALK, which provides a theoretical basis for previous research. We recommend DALK for patients with KC based on superior outcomes for postoperative corneal biomechanics.

Two types of DALK exist, namely, pd-DALK ($\geq$75%) and d-DALK.[7,9] Anwar,[47] who first introduced the concept of DALK, noted that dissection of host tissue close to the DM could lead to the formation of a smooth and transparent recipient bed, with functional outcomes similar to those following PK. There is a consensus that d-DALK and PK are the best surgical techniques for restoration of best uncorrected visual acuity in KC patients.[6] Ardjomand et al.[12]

compared visual function after DALK and PK in 23 patients with KC and concluded that RST affected visual function after DALK. They suggested that the visual acuity of KC eyes with RST less than 20 μm was comparable to that of PK. Further, comparisons of visual acuity following pd-DALK and d-DALK have revealed a lack of significant differences in visual acuity between the two groups, although eyes in the d-DALK group tended to exhibit more rapid visual recovery.[7,13,14] Sarnicola et al.[48] suggested that residual stroma may prevent perforation. Marchini et al.[15] intentionally retained a minimal stromal thickness of 50 μm to reduce the risk of DM rupture. Herein, we observed that an increase in RST (with the exception of a RST of 0 μm) resulted in greater corneal deformation and attenuation of VM stress in the healing zone following ideal-type DALK. Displacement and VM stress of the ideal-type DALK with a RST of 50 μm were the smallest, potentially because the ideal-type DALK assumed a uniform total corneal thickness of 560 μm, and graft thickness decreased with an increase in RST. In this regard, a greater amount of remaining diseased tissue in patients was associated with less depth of the peripheral healing zone. We concluded that RST has a greater impact on postoperative corneal biomechanical strength than on the healing zone when the total postoperative central corneal thickness (CCT) is constant; that is, greater RST is associated with weaker corneal biomechanics. We therefore recommend an RST of 50 μm for ideal-type DALK based on corneal stability.

In reality, accurate production of grafts of different thicknesses is challenging, which limits the clinical development of ideal-type DALK. In clinical settings such as advanced microkeratome instrumentation, excimer laser, and femtosecond laser, different RSTs can be achieved in recipients. A full-thickness donor button without DM and endothelium (500 μm) is positioned in the recipient bed with interrupted sutures. Therefore, postoperative cornea thickness is predominantly affected by RST. In our research, we observed that corneal deformation and VM stress after clinical-type DALK decreased with an increase in RST in both healing and optical zones. We speculate that the postsurgical increase in overall thickness is a major contributor to postoperative stability, which is consistent with the findings of Chen et al.[49] Ardjomand et al.[12] demonstrated that visual acuity after DALK with RST less than 20 μm was comparable to that after PK, whereas visual acuity was significantly reduced with a RST greater than 80 μm. Therefore, we recommend that RST should be retained as high as possible in clinical-type DALK based on the premise that postoperative visual acuity remains unaffected. In this

regard, future studies should investigate the effects of RST on vision. We can see that the change of VM stress distribution and deformation distribution of cornea is relatively special when RST = 0 in DALK. Herein, the calculation of the VM stress and deformation on the posterior surface of the cornea are extracted from the elements at the junction of the corneal stroma and the DM. The connection modes of elements between corneal stroma and DM differed with regard to the contact connection in the RST = 0 group and common node in other RST group (50, 100, 150, and 200 μm), which will mainly affect the VM stress and deformation distribution of the cornea.

In addition to the effect of RST in DALK on corneal biomechanics, IOP levels also affect corneal displacement and VM stress distribution. Herein, the IOP increased by approximately 5 mmHg, resulting in a 2.8-μm increase in the displacement of the apex of the posterior corneal surface (normal group). Regarding clinical-type DALK with a RST of 50 μm and PK, the increases in displacement were 3.08 μm and 3.17 μm, respectively. A previous study indicated that an IOP increase of 1 mmHg led to a decrease of 4.5 μm in the corneal radius of curvature,[3] which was higher than the value observed in this study. Differences in models and parameters may have underpinned this discrepancy. Our results indicate that corneal deformation after DALK and PK is slightly sensitive to IOP levels compared with that in the normal cornea.

In conclusion, we numerically analyzed corneal biomechanics after DALK and PK in this study. We have provided a theoretical description of the effects of RST in DALK and IOP on postoperative corneal biomechanics and demonstrated that DALK was more stable than PK. When the total postoperative CCT was constant (ideal-type DALK), an increase in RST was associated with decreased postoperative corneal biomechanics in the healing zone. When the graft CCT was constant (clinical-type DALK), corneal deformation and VM stress decreased with an increase in RST in both the healing and optical zones. Finally, IOP levels did not significantly influence corneal displacement and VM stress. The present FEM study provides a robust numerical simulation of corneal biomechanics after DALK and PK and offers novel insights into the optimal design for corneal transplantation in patients with KC. However, the modeling process still has limitations related to the accuracy of its assumptions. The setting of constitutive parameters for each layer of cornea may be an important influencing factor. Also, the exact dimensions and distribution of keratoconus zone are not known and were assumed to be circular, symmetric, and centered in this study. For this reason, future modeling still must be optimized.

Acknowledgments

References

1. Meek KM, Quantock AJ. The use of X-ray scattering techniques to determine corneal ultrastructure. *Prog Retin Eye Res*. 2001;20(1):95–137.
2. Meek KM, Tuft SJ, Huang YF, et al. Changes in collagen orientation and distribution in keratoconus corneas. *Invest Ophthalmol Vis Sci*. 2005;46(6):1948–1956.
3. Gefen A, Shalom R, Elad D, Mandel Y. Biomechanical analysis of the keratoconic cornea. *J Mech Behav Biomed Mater*. 2009;2(3):224–236.
4. Andreassen TT, Simonsen AH, Oxlund H. Biomechanical properties of keratoconus and normal corneas. *Exp Eye Res*. 1980;31(4):435–441.
5. Nash IS, Greene PR, Foster CS. Comparison of mechanical properties of keratoconus and normal corneas. *Exp Eye Res*. 1982;35(5):413–424.
6. Gomes JAP, Tan D, Rapuano CJ, et al. Global consensus on keratoconus and ectatic diseases. *Cornea*. 2015;34(4):359–369.
7. Spadea L, De Rosa V. Current techniques of lamellar keratoplasty for keratoconus. *Saudi Med J*. 2016;37(2):127–136.
8. Tan DTH, Dart JKG, Holland EJ, Kinoshita S. Corneal transplantation. *Lancet*. 2012;379(9827):1749–1761.
9. Lu Y, Grisolia ABD, Ge YR, et al. Comparison of femtosecond laser-assisted descemetic and predescemetic lamellar keratoplasty for keratoconus. *Indian J Ophthalmol*. 2017;65(1):19–23.
10. Bergmanson JPG, Goosey JD, Patel CK, Matthew JH. Recurrence or re-emergence of keratoconus-what is the evidence telling us? Literature review and two case reports. *Ocul Surf*. 2014;12(4):267–272.
11. Feizi S, Javadi MA, Khajuee-Kermani P, Jafari R. Repeat keratoplasty for failed deep anterior lamellar keratoplasty in keratoconus: incidence, indications, and outcomes. *Cornea*. 2017;36(5):535–540.
12. Ardjomand N, Hau S, McAlister JC, et al. Quality of vision and graft thickness in deep anterior lamellar and penetrating corneal allografts. *Am J Ophthalmol*. 2007;143(2):228–235.
13. Abdelkader A, Kaufman HE. Descemetic versus pre-descemetic lamellar keratoplasty: clinical and confocal study. *Cornea*. 2011;30(11):1244–1252.
14. Sarnicola V, Toro P, Gentile D, Hannush SB. Descemetic DALK and predescemetic DALK: outcomes in 236 cases of keratoconus. *Cornea*. 2010;29(1):53–59.
15. Marchini G, Mastropasqua L, Pedrotti E, Nubile M, Ciancaglini M, Sbabo A. Deep lamellar keratoplasty by intracorneal dissection: a prospective clinical and confocal microscopic study. *Ophthalmology*. 2006;113(8):1289–1300.
16. Sarnicola V, Toro P, Sarnicola C, Sarnicola E, Ruggiero A. Long-term graft survival in deep anterior lamellar keratoplasty. *Cornea*. 2012;31(6):621–626.
17. Hosny M, Hassaballa MAM, Shalaby A. Changes in corneal biomechanics following different keratoplasty techniques. *Clin Ophthalmol*. 2011;5:767–770.
18. Ziaei M, Vellara HR, Gokul A, Ali NQ, McGhee CNJ, Patel DV. Comparison of corneal biomechanical properties following penetrating keratoplasty and deep anterior lamellar keratoplasty for keratoconus. *Clin Exp Ophthalmol*. 2020;48(2):174–182.
19. Jiang MS, Zhu JY, Li X, Zhang NN, Zhang XD. Corneal biomechanical properties after penetrating keratoplasty or deep anterior lamellar keratoplasty using the ocular response analyzer: a meta-analysis. *Cornea*. 2017;36(3):310–316.
20. Maeda N, Ueki R, Fuchihata M, Fujimoto H, Koh S, Nishida K. Corneal biomechanical properties in 3 corneal transplantation techniques with a dynamic Scheimpflug analyzer. *Jpn J Ophthalmol*. 2014;58(6):483–489.
21. Jafarinasab MR, Feizi S, Javadi MA, Hashemloo A. Graft biomechanical properties after penetrating keratoplasty versus deep anterior lamellar keratoplasty. *Curr Eye Res*. 2011;36(5):417–421.
22. Abdelkader A. Influence of different keratoplasty techniques on the biomechanical properties of the cornea. *Acta Ophthalmol*. 2013;91(7):e567–e572.
23. Roy AS, Dupps WJ, Roberts CJ. Comparison of biomechanical effects of small-incision lenticule extraction and laser in situ keratomileusis: finite-element analysis. *J Cataract Refract Surg*. 2014;40(6):971–980.
24. Mohamed S, Coccarelli A, Mauro A, et al. A novel numerical modelling approach for keratoplasty

eye procedure. *Biomech Model Mechanobiol*. 2019;18(5):1429–1442.

25. Khan SN, Shiakolas PS. Finite element analysis of Descemet's stripping automated endothelial keratoplasty (DSAEK) surgery allograft to predict endothelial cell loss. *Curr Eye Res*. 2017;42(1):32–40.

26. Roy AS, Dupps WJ. Patient-specific computational modeling of keratoconus progression and differential responses to collagen cross-linking. *Invest Ophthalmol Vis Sci*. 2011;52(12):9174–9187.

27. Djotyan GP, Soong HK, Mian S, Fernández DC, Kurtz RM, Juhasz T. Finite-element modeling of posterior lamellar keratoplasty: construction of theoretical nomograms for induced refractive errors. *Ophthalmic Res*. 2006;38(6):329–334.

28. Kling S, Marcos S. Finite-element modeling of intrastromal ring segment implantation into a hyperelastic cornea. *Invest Ophthalmol Vis Sci*. 2013;54(1):881–889.

29. Ma JN, Wang Y, Wei PH, Jhanji V. Biomechanics and structure of the cornea: implications and association with corneal disorders. *Surv Ophthalmol*. 2018;63(6):851–861.

30. Anderson K, El-Sheikh A, Newson T. Application of structural analysis to the mechanical behaviour of the cornea. *J R Soc Interface*. 2004;1(1):3–15.

31. Su P, Lu DA, Deng SJ, Zhang LY, Hao YX, Yang Y. Three-dimensional biomechanical modeling and simulation of trephine cutting cornea for keratoplasty. *Acta Bioeng Biomech*. 2018;20(2):23–33.

32. Randleman JB, Dawson DG, Grossniklaus HE, McCarey BE, Edelhauser HF. Depth-dependent cohesive tensile strength in human donor corneas: implications for refractive surgery. *J Refract Surg*. 2008;24(1):S85–S89.

33. Ruberti JW, Roy AS, Roberts CJ. Corneal biomechanics and biomaterials. *Annu Rev Biomed Eng*. 2011;13:269–295.

34. Pinsky PM, Heide DVD, Chernyak D. Computational modeling of mechanical anisotropy in the cornea and sclera. *J Cataract Refract Surg*. 2005;31(1):136–145.

35. Hatami-Marbini H. Hydration dependent viscoelastic tensile behavior of cornea. *Ann Biomed Eng*. 2014;42(8):1740–1748.

36. Pandolfi A, Manganiello F. A model for the human cornea: constitutive formulation and numerical analysis. *Biomech Model Mechanobiol*. 2006;5(4):237–246.

37. Elsheikh A, Wang DF. Numerical modelling of corneal biomechanical behaviour. *Comput Methods Biomech Biomed Engin*. 2007;10(2):85–95.

38. Yu J-G, Bao F-J, Joda A, et al. Influence of glucocorticosteroids on the biomechanical properties of in-vivo rabbit cornea. *J Mech Behav Biomed Mater*. 2014;29:350–359.

39. Alastrué V, Calvo B, Peña E, Doblaré M. Biomechanical modeling of refractive corneal surgery. *J Biomech Eng*. 2006;128(1):150–160.

40. Fraldi M, Cutolo A, Esposito L, Guarracino F. The role of viscoelasticity and stress gradients on the outcome of conductive keratoplasty. *Biomech Model Mechanobiol*. 2011;10(3):397–412.

41. Bao FJ. *Clinical verification of predicting tools for laser in situ keratomileusis and construction of ocular biomechanical measurement platform*. Wenzhou, China: Wenzhou Medical University, 2015.

42. Simonsen AH, Andreassen TT, Bendix K. The healing strength of corneal wounds in the human eye. *Exp Eye Res*. 1982;35(3):287–292.

43. Pandolfi A, Fotia G, Manganiello F. Finite element simulations of laser refractive corneal surgery. *Eng Comput*. 2009;25(1):15–24.

44. Bukowiecki A, Hos D, Cursiefen C, Eming SA. Wound-healing studies in cornea and skin: parallels, differences and opportunities. *Int J Mol Sci*. 2017;18(6):1257.

45. Cintron C, Covington HI, Kublin CL. Morphologic analyses of proteoglycans in rabbit corneal scars. *Invest Ophthalmol Vis Sci*. 1990;31(9):1789–1798.

46. Foroutan AR, Gheibi GH, Joshaghani M, Ahadian A, Foroutan P. Traumatic wound dehiscence and lens extrusion after penetrating keratoplasty. *Cornea*. 2009;28(10):1097–1099.

47. Anwar M. Dissection technique in lamellar keratoplasty. *Br J Ophthalmol*. 1972;56:711–713.

48. Sarnicola V, Toro P, Sarnicola C, Sarnicola E, Ruggiero A. Long-term graft survival in deep anterior lamellar keratoplasty. *Cornea*. 2012;31(6):621–626.

49. Chen XG, Shen M, Wang Y, Wu D, Zhang L. Finite element analysis of corneal deformation and stress after LASIK. *Chin J Optom Ophthalmol Vis Sci*. 2019;21(2):110–116.